Ab initio study of helium in α-Fe: Dissolution, migration, and clustering with vacancies

Chu-Chun Fu and F. Willaime
Service de Recherches de Métallurgie Physique, CEA/Saclay, 91191 Gif-sur-Yvette Cedex, France
(Received 7 January 2005; revised manuscript received 13 July 2005; published 24 August 2005)

Density functional theory calculations have been performed to study the dissolution and migration of helium in α-iron, and the stability of small helium-vacancy clusters He_nV_m $(n,m=0$ to 4). Substitutional and interstitial configurations of helium are found to have similar stabilities. The tetrahedral configuration is more stable than the octahedral by 0.2 eV. Interstitial helium atoms are predicted to have attractive interactions and a very low migration energy (0.06 eV), suggesting that He bubbles can form at low temperatures in initially vacancy-free lattices. The migration of substitutional helium by the vacancy mechanism is governed by the migration of the HeV_2 complex, with an energy barrier of 1.1 eV. The activation energies for helium diffusion by the dissociation and vacancy mechanisms are estimated for the limiting cases of thermal-vacancy regime and of high supersaturation of vacancies. The trends of the binding energies of vacancy and helium to helium-vacancy clusters are discussed in terms of providing additional knowledge on the behavior of He in irradiated iron, necessary for the interpretation of complex experimental data such as thermal He desorption spectra.

DOI: 10.1103/PhysRevB.72.064117 PACS number(s): 71.15.Mb, 75.20.En, 71.15.Nc, 66.30.Jt

I. INTRODUCTION

Ferritic steels are proposed as structural material in fusion reactors. When subject to 14 MeV neutron irradiation, large amounts of helium and hydrogen are produced from (n,α) transmutation reactions in addition to self-defects. High He concentrations are known to induce bubble formation[1] and void swelling.[2] Changes in the microstructural and mechanical properties, such as high temperature embrittlement, surface roughening, and blistering, have also been evidenced.[1,3] The atomistic properties of helium in metals at the origin of these phenomena are difficult to identify from experiments. Thermal desorption after He irradiation or implantation yields information on He migration and the stability of He_nV_m clusters, but the interpretation of these data is not free of ambiguities.[4,5] The energetics of the elementary mechanisms which come into play are mainly known from atomistic simulations performed using empirical potentials (EPs).[1,6] The main results reported in α-iron are summarized in Refs. 7–9. The accuracy of these predictions is questioned by very recent *ab initio* calculations which show that the relative stabilities of the various He solution sites are not correctly reproduced by existing EPs.[10] In the absence of experimental validation, a broader *ab initio* database on the energetics of He in iron is therefore needed. Here we present the results of *ab initio* studies on helium solution sites, the possible migration mechanisms and barriers of interstitial and substitutional He, and the stability of small helium-vacancy complexes.

II. METHOD OF CALCULATION

The present calculations have been performed within the density functional theory (DFT) as implemented in the SIESTA code.[11] The calculations are spin polarized and use the generalized gradient approximation (GGA). Core electrons are replaced by nonlocal norm-conserving pseudopotentials. Valence electrons are described by linear combinations of numerical pseudo-atomic orbitals. The pseudopotential and the basis set for Fe atoms are the same as in Ref. 12. The cutoff radius for the pseudopotential of He is set to 0.52 Å, and its basis set consists of localized functions with a cutoff radius of 3.22 Å with two functions for the $1s$ state and three for the $2p$ states, included as polarized orbitals in order to increase angular flexibility. The charge density is represented on a regular real space grid of 0.078 Å.

The present approach was shown to successfully account for the properties of self-defects in iron.[12] The accuracy of the description of the He-He interaction is tested on the energy of an isolated He dimer calculated in the range of interatomic distances from 1.5 to 4 Å, the shortest distance between He atoms involved in the present study being 1.6 Å. First, an excellent agreement is obtained with a similar DFT-GGA calculation performed with a plane wave basis set using the PWSCF code[13] attesting for the validity of the present basis set (Fig. 1). However the van der Waals interactions—which govern the weak binding between isolated He atoms—are not explicitly taken into account within DFT-GGA. We have therefore performed a comparison with a set of more accurate calculations: full configuration interaction (CI) calculations[14] for interatomic distances from 2 to 6 Å, and quantum Monte Carlo (QMC) calculations[15] for smaller distances. The largest absolute difference with these reference calculations is only 0.03 eV; it is obtained for the smallest distances (Fig. 1). This discrepancy is small compared to the interaction energies determined in this work. Note that close to the minimum of the binding energy curve the discrepancy becomes larger in relative values but it is completely negligible in absolute values (0.002 eV) compared to the accuracy needed in the present calculations. Finally, concerning Fe-He interactions, DFT-GGA was shown to successfully describe, e.g., the interaction of He with various metallic surfaces.[16,17]

Supercell calculations are performed to study the defect properties. Except as otherwise noted, all the results reported here have been obtained on 128 atom cells using a $3\times3\times3$ k-point grid and the Methfessel-Paxton broadening scheme with a 0.3 eV width. The structures are optimized by

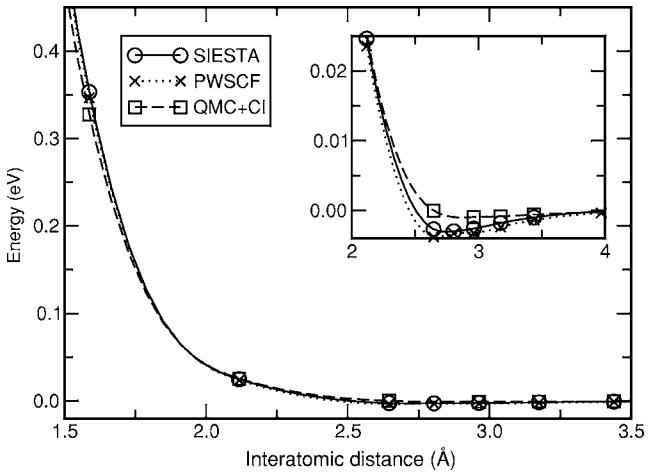

FIG. 1. Helium-helium interaction energy within an isolated He dimer for the interatomic distances involved in the present study: comparison between the present SIESTA and PWSCF (Ref. 13) DFT-GGA calculations and reference QMC (Ref. 15) and full CI (Ref. 14) results (below and above 2 Å, respectively). The inset shows the behavior around the equilibrium distance.

relaxing both the atomic positions and the shape and volume of the supercell. The migration paths are calculated using the drag method: the atomic positions relative to the center of mass are constrained to relax in the hyperplane perpendicular to the vector connecting the initial and final positions. An important quantity in the following is the binding energy of a defect (a vacancy or an interstitial He) to a He_nV_m complex [$E^b(V-He_nV_m)$ and $E^b(He_{int}-He_nV_m)$]. It is defined as the energy difference between the situations where the defect is infinitely separated from the complex and where it is added to the complex, making respectively a $He_{n+1}V_m$ and a He_nV_{m+1} complex.[8,18]

III. RESULTS

A. Dissolution of He in α-iron

The relative stabilities of the various helium insertion sites are determined by calculating the solution energies of the substitutional and high symmetry interstitial sites. For a supercell containing N Fe atoms and one He atom, with energy $E(N\text{Fe},\text{He})$, the solution energy is calculated as $E^{sol}=E(N\text{Fe},\text{He})-NE(\text{Fe})-E(\text{He})$, where $E(\text{Fe})$ and $E(\text{He})$ are the energies per Fe atom in a bcc lattice and of an isolated He, respectively. The values obtained for the substitutional, tetrahedral, and octahedral sites are shown in Table I for various calculation conditions: they are found to depend very weakly on the supercell size, the k-point grid, and the real-space grid-spacing showing that these energies are very well converged with respect to these sources of error. The present results are also in very good agreement with the DFT-GGA values reported using the VASP plane-wave code[10] attesting to the validity of the present approach (see Table I). These *ab initio* solution energies differ significantly from those obtained with empirical potentials (3.25, 5.34, and 5.25 eV for the substitutional, tetrahedral, and octahedral sites, respectively).[7] As a consequence the predicted preferential interstitial site is tetrahedral instead of octahedral with EPs, but more importantly a much smaller value is predicted for the energy difference between substitutional and interstitial solution energies, or equivalently the He_{int}-vacancy binding energy (2.3 eV here against 3.7 eV with EP), as summarized in Table II.

TABLE I. Solution energies of helium in iron calculated at constant pressure. Comparison between the present SIESTA calculations using 54 and 128 atom cells and plane wave VASP results (Ref. 10). The SIESTA values are shown for various real-space grid-spacings (expressed in Å) and k-point grids. All the energies are in electron volts

	Real space grid	k points	E^{sol}_{sub}	E^{sol}_{tetra}	E^{sol}_{octa}
54 atom cell					
SIESTA	0.078	$6\times6\times6$	4.19	4.38	4.55
128 atom cell					
SIESTA	0.078	$3\times3\times3$	4.22	4.39	4.57
SIESTA	0.064	$3\times3\times3$	4.22	4.39	4.58
SIESTA	0.078	$4\times4\times4$	4.23	4.40	4.58
VASP			4.08	4.37	4.60

In order to understand the above discrepancies between *ab initio* and EP results, we have examined the possible changes in magnetism caused by He insertion. We have identified the local magnetic moments on Fe or He atoms, μ^{Fe} and μ^{He}, obtained from a Mulliken population analysis. Unlike the cases of C and N,[19] He atoms do not become magnetic in either substitutional or interstitial sites ($|\mu^{He}| \leqslant 0.05\ \mu_B$), as expected from the fact that no hybridization occurs between the closed 1s shells of He and the iron valence band. The local magnetic moments around a vacancy increase with respect to the bulk value of 2.31 μ_B by 0.23 μ_B, due to the decrease in number of nearest neighbors, but they are then practically unchanged when a helium atom is introduced ($|\Delta\mu^{Fe}| \leqslant 0.02\ \mu_B$). Similarly, the magnetic moments of the first neighbors of interstitial He increase only weakly: $\Delta\mu^{Fe}=+0.09\ \mu_B$ and $+0.03\ \mu_B$ for the tetrahedral

TABLE II. Solution properties of He in α-iron. Comparison between *ab initio* SIESTA and previous empirical potential (EP) results on the solution energies in the substitutional site, E^{sol}_{sub}, the preferential interstitial site, the difference between solution energies in the substitutional and the tetrahedral ($E^{sol}_{tetra}-E^{sol}_{sub}$), and between the tetrahedral and the octahedral sites ($E^{sol}_{octa}-E^{sol}_{tetra}$), and the binding energy between an interstitial He and a vacancy, $E^b(He_{int}-V)$. All the energies are in electron volts.

Property	Present work	EP (Ref. 7)
E^{sol}_{sub}	4.22	3.25
Preferential interstitial site	tetrahedral	octahedral
$E^{sol}_{tetra}-E^{sol}_{sub}$	0.17	2.09
$E^{sol}_{octa}-E^{sol}_{tetra}$	0.18	−0.09
$E^b(He_{int}-V)$	2.30	3.70

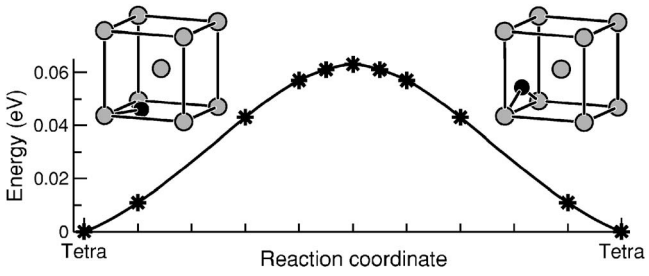

FIG. 2. Energy barrier for the migration of an interstitial He atom. Initial and final configurations are schematically represented with black and gray spheres for He and Fe atoms, respectively.

and octahedral sites, respectively, which is negligible compared to the decrease observed in the case of C and N ($\Delta\mu^{\mathrm{Fe}}=-0.65\ \mu_B$).[19] As a conclusion, the changes in the electronic structure of Fe induced by the insertion of He produce weak effects on the magnetization of Fe, as compared to other impurities or self-interstitials.[20] There is therefore no evidence of a direct magnetic effect on the relative stabilities of He insertion sites. Further studies are required to find out the real origin of the discrepancies in He solution energies between the two models.

B. Migration of interstitial and substitutional He

Concerning the kinetics of He in bcc iron, we first examine the case of interstitial He migration, which is relevant to the initial stage after He implantation or He production by transmutation. A tetrahedral solute may migrate between two equivalent sites without passing through an octahedral one (Fig. 2), as reported, e.g., in the case of H in iron.[21] A very low migration energy, $E^m(\mathrm{He_{int}})=0.06$ eV, is found here for He with this three-dimensional mechanism. Such a low migration energy means that the migration of interstitial He is almost athermal. Note that the EP value is similar, namely 0.08 eV, despite the discrepancy between the two models on the site preference for interstitial He.[8]

We now turn to the migration of substitutional He, which may occur mainly either by vacancy or by dissociation mechanisms.[22,23] The first mechanism requires another incoming vacancy. We find that the most stable configuration for the HeV_2 complex is when the two vacancies are first neighbors with a vacancy to substitutional He binding energy of 0.78 eV, followed by the configuration where they are second neighbors, with a binding energy of 0.37 eV. Note that the relative stability of the first and second neighbor configurations is reversed with respect to the case of the divacancy without helium.[7,12] The interaction between a substitutional He and a vacancy becomes negligible at third neighbor distance. Concerning the position of the helium atom, it is located midway between the two vacancies in the nearest neighbor case [(c) in Fig. 3]. This configuration is very stable as attested by the fact that when the helium atom is forced to be on the substitutional site, the energy—after relaxation with a proper constraint—increases by 0.47 eV with respect to the minimum value. For the second neighbor case, the helium atom also prefers to be off-site and it can adopt two energetically equivalent positions, located at 0.25

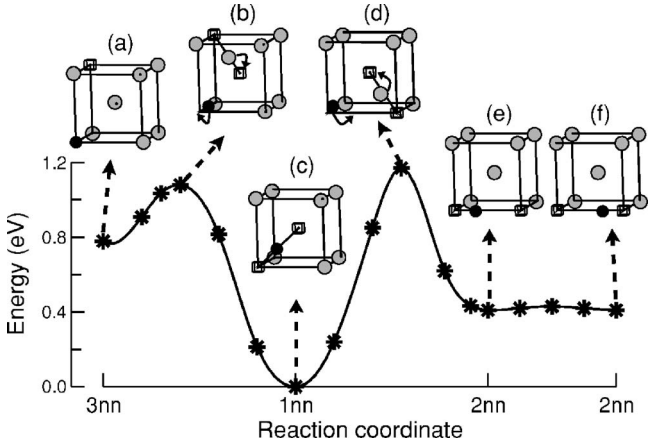

FIG. 3. Schematic representation of the energy landscape of the HeV_2 complex: (c) ground state configuration with a helium atom bound to two nearest-neighbor vacancies; (e) second and (a) third neighbor configurations; (b) and (d) saddle point configurations; and (f) other equivalent second neighbor configuration. The solid arrows in (b) and (d) indicate atomic jumps yielding configurations (a) and (e), respectively, starting from (c). The atoms (black spheres for He and gray spheres for Fe) are represented at their relaxed positions. Vacancies are symbolized by small cubes.

times the lattice parameter from either of the two vacancies [(e) and (f) in Fig. 3], and separated by a barrier of 0.02 eV. For the third neighbor case, the helium atom sits on one of the two vacancies [(a) in Fig. 3].

From the first, second, and third neighbor arrangements two competing two-step migration mechanisms are proposed for the HeV_2 complex (Fig. 3). The first one involves a second neighbor intermediate configuration [(e) in Fig. 3]. First, a nearest neighbor jump of the vacancy transforms the nearest neighbor configuration into a second neighbor one; in the saddle point configuration He occupies a substitutional site [(d) in Fig. 3]. Then, by a similar but reverse jump, a nearest neighbor configuration is recovered. The corresponding migration energy is 1.17 eV. The second mechanism involves the third neighbor intermediate configuration [(a) in Fig. 3]; this configuration is higher in energy but actually has a slightly lower barrier (1.08 eV). These barriers are lower than the lower bound value of the vacancy from HeV_2 dissociation energy (1.45 eV), estimated from the sum of the vacancy to $\mathrm{He_{sub}}$ binding energy and the vacancy migration energy (0.67 eV). Therefore the HeV_2 complex is expected to migrate as a unit over appreciable distances via substitutional He vacancy mechanisms.

We have completed the analysis of the migration paths for the migrations of interstitial He and of HeV_2 via the third neighbor configuration by performing a calculation of the vibrational modes at the respective saddle points.[24] In both cases only one negative eigenvalue of the Hessian matrix is found, indicating that these saddle points are of order one.[25] Therefore there is no possibility to decay to local minima other than those considered here starting from these saddle points.

Assuming an Arrhenius dependence for the substitutional He diffusion, effective migration energies can be defined for the vacancy mechanisms described above and the dissocia-

TABLE III. Effective migration energies (in eV) of substitutional He in α-iron. Comparison between the dissociation and vacancy mechanisms: (a) when thermal vacancies dominate and (b) when there is a supersaturation of vacancies. The expressions for the dissociation mechanism are taken from Ref. 5. For the vacancy case they are derived from Ref. 26, where $E^m(\mathrm{He}V_2)$ is the migration energy of the $\mathrm{He}V_2$ complex—taken here as the barrier from first to third neighbor configurations—and $E^b(V-\mathrm{He}_{\mathrm{sub}})$ is the binding energy of a vacancy to a substitutional He.

	By dissociation	
(a)	$E^b(\mathrm{He}_{\mathrm{int}}-V)+E^m(\mathrm{He}_{\mathrm{int}})-E^f(V)$	0.24
(b)	$E^b(\mathrm{He}_{\mathrm{int}}-V)+E^m(\mathrm{He}_{\mathrm{int}})$	2.36
	By vacancies	
(a)	$E^m(\mathrm{He}V_2)+E^f(V)-E^b(V-\mathrm{He}_{\mathrm{sub}})$	2.42
(b)	$E^m(\mathrm{He}V_2)-E^b(V-\mathrm{He}_{\mathrm{sub}})$	0.30

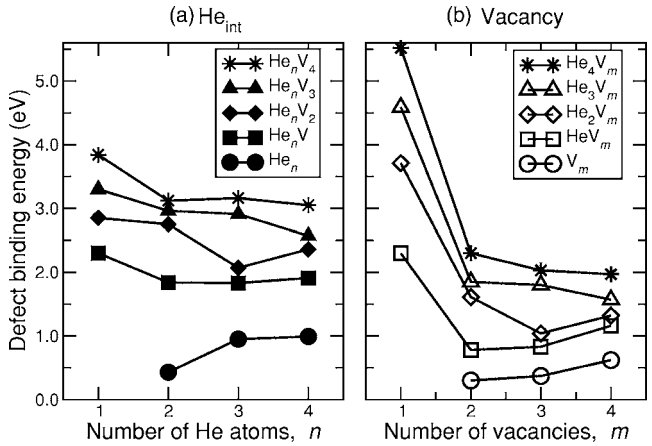

FIG. 4. Binding energies of (a) a $\mathrm{He}_{\mathrm{int}}$ atom and (b) a vacancy to a $\mathrm{He}_{n-1}V_m$ and He_nV_{m-1} cluster, respectively. The abscises and the legends refer to the compositions of the resulting clusters.

tion one, i.e., when a substitutional He dissociates from its vacancy to migrate through interstitial sites until it is trapped by another defect. Two limiting regimes can be distinguished, depending on whether vacancies are present at their thermal equilibrium concentration, or if they are highly supersaturated, as it is the case under irradiation at low to intermediate temperature. The expressions for these effective migration energies[5,26] and the values obtained from the present calculations are summarized in Table III. A wide range of values are obtained. If thermal vacancies prevail, their concentration is governed by the vacancy formation energy, $E^f(V)$—this explains why $E^f(V)$ enters in the expressions of the effective migration energies—and we find that the dominant diffusion mechanism is expected to be dissociative. When vacancies are supersaturated, i.e., when irradiation-induced vacancies dominate, no general conclusion can be drawn because the vacancy concentration C_v is a constant that depends on the initial irradiation conditions. C_v enters in different ways into the preexponential factors for vacancy and dissociation mechanisms,[5] therefore a crossover as function of temperature may occur. Note that EP studies[7,8] give larger effective migration energies by dissociation, that is, 2.08 and 3.78 eV instead of 0.24 and 2.36 eV, respectively, mainly because the predicted $\mathrm{He}_{\mathrm{int}}-V$ binding energy is larger. From desorption experiments after implantation[5] He migration was interpreted to occur by dissociation with an energy barrier of 1.4 ± 0.3 eV, i.e., smaller than our calculated value of 2.36 eV. In view of the complexity of experimental conditions, e.g., the presence of a large variety of helium-vacancy defects and residual impurities, as well as the simplicity of both experimental data analysis and the present assumptions, further investigations are required to clarify this discrepancy.

C. Stability of small helium-vacancy clusters

The stability of small He_nV_m clusters was also investigated for n and $m=0$ to 4. The vacancy and $\mathrm{He}_{\mathrm{int}}$ binding energies to the clusters are found to be positive in all cases, i.e., all interactions are attractive (Fig. 4). The He binding energies are positive even in absence of vacancies ($m=0$). This self-trapping of He atoms, together with the fast migration of interstitial He, was proposed to be responsible for the formation of He bubbles observed at low temperatures in Au in initially vacancy-free lattices.[27] For $n=1$, the $\mathrm{He}_{\mathrm{int}}$ binding energy increases as a function of the number of vacancies in the cluster, m; it tends rapidly to the asymptotic value of interstitial He solution energy, i.e., 4.39 eV in the present calculation. For a given value of m, the He binding energy decreases as the He content increases, reflecting the increase in cluster pressure caused by the accumulation of He atoms. Empirical potentials show the same trend,[8] and predict a spontaneous emission of He or self-interstitials at larger n/m ratios.

The vacancy to cluster binding energies increase with helium content—again as a consequence of the increase of cluster pressure—and in particular they are always larger with than without helium [Fig. 4(b)]. In other words helium stabilizes vacancy-type clusters by reducing the vacancy emission rates.[8] This is consistent with the experimental evidence that He atoms enhance the formation of microvoids.[2] For a given number of He atoms, n, the vacancy binding energy first decreases rapidly when the number of vacancies increases, until $m-1\simeq n$, i.e., until the cluster pressure becomes small enough. Then it increases slowly (as in the helium-free case), when the cluster surface-energy contribution becomes dominant; the asymptotic value for all curves is the monovacancy formation energy, i.e., 2.12 eV in the present calculation.

The defect to cluster binding energy was shown to depend strongly on the He density, i.e., the n/m ratio.[8] Clusters may change their n/m ratio by, e.g., emitting He atoms or vacancies according to their respective dissociation energies. The *ab initio* trend for the He dissociation energies from He_nV_m clusters is shown in Figure 5 as a function of n/m, assuming that this is the sum of the binding energy to the cluster and the interstitial He migration energy.[8] Fig. 5 also shows the vacancy dissociation energies calculated in a similar fashion. In the thermal helium desorption spectroscopy (THDS) experiment, dissociation reactions with increasing activation

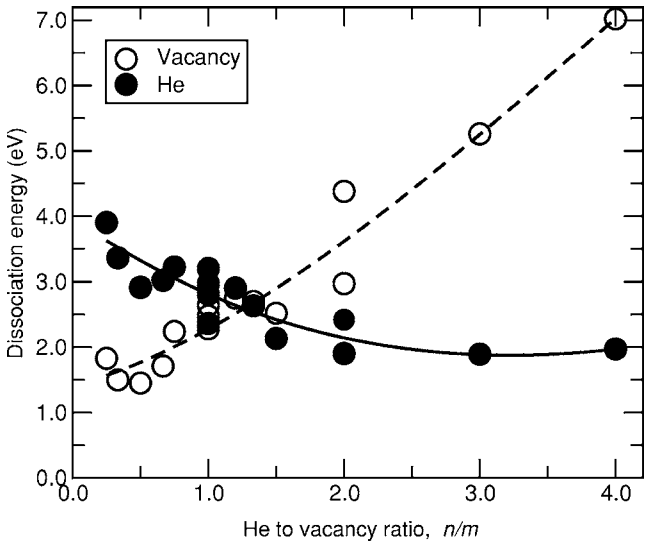

FIG. 5. Dissociation energies of a He atom or a vacancy from He_nV_m clusters as a function of He to vacancy ratio.

energies can be obtained as temperature increases. The crossover between the He and vacancy dissociation curves therefore gives information on the composition of the most stable clusters and on their stability.[8] In the present calculation the crossover corresponds to $n/m \simeq 1.3$, and $E^{\mathrm{dis}} \simeq 2.6$ eV, while EPs predict $n/m \simeq 1.8$ and $E^{\mathrm{dis}} \simeq 3.6$ eV. This discrepancy and in general the discrepancies between EPs and *ab initio* dissociation energies have a direct impact on the interpretation of the peaks observed at well-defined temperatures in THDS experiments.[4,6,28] For instance, the activation energy associated with peak II observed at around 750 K is estimated to be 2.4 ± 0.4 eV.[4] According to the present calculations the dissociation of a substitutional He from its vacancy, with an activation energy of 2.36 eV, is a very good candidate for this peak, whereas based on the EP value of 3.78 eV this dissociation event was proposed instead as one of the possible interpretations for peak III, occurring at around 1100 K.[4]

IV. CONCLUSIONS

The energetics and mobility of He in α-iron and the stability of small He_nV_m clusters have been revisited by *ab initio* calculations. The energy difference between He in the substitutional site and in the tetrahedral configuration is found to be unexpectedly small compared to previous empirical potential estimations. This discrepancy is related to a significantly lower binding energy between a vacancy and an interstitial He, which implies a lower effective migration energy for substitutional He by the dissociation mechanism. Interstitial He atoms are found to have a very low migration energy and to attract each other, suggesting that He bubbles can form at low temperatures in initially vacancy-free lattices. The binding energies of an interstitial He or a vacancy to small helium-vacancy clusters have been calculated for clusters with up to four vacancies and four helium atoms; the trends are similar to previous empirical potential studies but quantitative discrepancies are evidenced such that important consequences are expected on the interpretation of THDS data.

ACKNOWLEDGMENTS

B.D. Wirth is acknowledged for careful reading of the manuscript. This work was funded by the European Fusion Materials Modelling Programme. Calculations have been performed at the CINES computing center (Montpellier, France).

[1] *Fundamental Aspects of Inert Gases in Solids*, edited by S. E. Donnelly and J. H. Evans (Plenum, New York, 1991).
[2] T. Ishizaki, Q. Xu, T. Yoshiie, S. Nagata, and T. Troev, J. Nucl. Mater. **307-311**, 961 (2002).
[3] H. Trinkaus and B. N. Singh, J. Nucl. Mater. **323**, 229 (2003) and references therein.
[4] K. Morishita, R. Sugano, H. Iwakiri, N. Yoshida, and A. Kimura, *Proc. 4th Pacific Rim Int. Conf. on Advanced Materials and Processing (PRICM4)*, The Japan Institute of Metals (2001), pp. 1395–1398.
[5] R. Vassen, H. Trinkaus, and P. Jung, Phys. Rev. B **44**, 4206 (1991).
[6] In *Properties and Interactions of Atomic Defects in Metals and Alloys*, edited by H. Ullmaier, Landolt Börnstein, New Series Group III, Vol. 25 (Springer-Verlag, Berlin, 1991), Chap. 3, p. 380.
[7] K. Morishita, B. D. Wirth, T. Diaz de la Rubia, and A. Kimura, *Proc. 4th Pacific Rim Int. Conf. on Advanced Materials and Processing (PRICM4)*, The Japan Institute of Metals (2001), pp. 1383–1386.
[8] K. Morishita, R. Sugano, B. D. Wirth, and T. Diaz de la Rubia, Nucl. Instrum. Methods Phys. Res. B **202**, 76 (2003).
[9] B. Wirth, G. R. Odette, J. Marian, L. Ventelon, J. A. Young-Vandersall, and L. A. Zepeda-Ruiz, J. Nucl. Mater. **329-333**, 103 (2004).
[10] T. Seletskaia, Y. Osetsky, R. E. Stoller, and G. M. Stocks, Phys. Rev. Lett. **94**, 046403 (2005).
[11] J. M. Soler, E. Artacho, J. D. Gale, A. Garcia, J. Junquera, P. Ordejón, and D. Sanchez-Portal, J. Phys.: Condens. Matter **14**, 2745 (2002).
[12] C. C. Fu, F. Willaime, and P. Ordejón, Phys. Rev. Lett. **92**, 175503 (2004); C. C. Fu, J. Dalla Torre, F. Willaime, J. L. Bocquet, and A. Barbu, Nat. Mater. **4**, 68 (2005).
[13] The DFT plane wave calculations are performed with the PWSCF package (S. Baroni, A. Dal Corso, S. de Gironcoli, and P. Giannozzi, http://www.pwscf.org) using an ultrasoft pseudopotential and an energy cutoff of 30 Ry.
[14] T. van Mourik and J. H. van Lenthe, J. Chem. Phys. **102**, 7479 (1995).
[15] D. M. Ceperley and H. Partridge, J. Chem. Phys. **84**, 821 (1986).

[16] M. Petersen, S. Wilke, P. Ruggerone, B. Kohler, and M. Scheffler, Phys. Rev. Lett. **76**, 995 (1996).
[17] N. Jean, M. I. Trioni, G. P. Brivio, and V. Bortolani, Phys. Rev. Lett. **92**, 013201 (2004).
[18] For example $E^b(\mathrm{V}-\mathrm{He}_n V_m)=E^f(V)+E^f(\mathrm{He}_n V_{m-1})-E^f(\mathrm{He}_n V_m)$, where $E^f(V)$ and $E^f(\mathrm{He}_n V_m)$ are the formation energies of a vacancy and a $\mathrm{He}_n V_m$ cluster.
[19] C. Domain, C. S. Becquart, and J. Foct, Phys. Rev. B **69**, 144112 (2004).
[20] C. Domain and C. S. Becquart, Phys. Rev. B **65**, 024103 (2001).
[21] D. E. Jiang and E. A. Carter, Phys. Rev. B **70**, 064102 (2004).
[22] L. K. Mansur, E. H. Lee, P. J. Maziasz, and A. P. Rowcliffe, J. Nucl. Mater. **141-143**, 633 (1986).
[23] J. B. Adams and W. G. Wolfer, J. Nucl. Mater. **158**, 25 (1988).
[24] These calculations were performed using a 54 atom cell with a $6\times6\times6$ k-point grid. The dynamical matrices were determined by the finite difference method applied to the forces.
[25] M. Nastar, V. V. Bulatov, and S. Yip, Phys. Rev. B **53**, 13521 (1996).
[26] V. Sciani and P. Jung, Radiat. Eff. **78**, 87 (1988).
[27] G. Thomas and R. Bastasz, J. Appl. Phys. **52**, 6426 (1981).
[28] E. V. Kornelsen, Radiat. Eff. **13**, 227 (1972).